

A Novel family of H6 Transformer less Full-Bridge PV Grid-Tied Inverters

Lavanya Rallapalli¹, S.Ramesh²

PG Student [PE&ED], Dept. of EEE, SISTK, rallapalli.lavanya7@gmail.com,India¹

Associative professor, Dept. of EEE, SISTK,Swamiramesh20@gmail.com,Andhra Pradesh, India²



Abstract—Transformer less inverters are widely utilized in grid-tied photovoltaic (PV) generation systems, due to the benefits of achieving high efficiency and low cost. Sundry transformer less inverter topologies have been proposed to meet the safety requisite of leakage currents, such as designated in the VDE-4105 standard. In this paper, a family of H6 transformer less inverter topologies with low leakage currents is proposed, and the intrinsic relationship between H5 topology, highly efficient and reliable inverter concept (HERIC) topology, and the proposed H6 topology has been discussed as well. One of the proposed H6 inverter topologies is taken as an example for detail analysis with operation modes and modulation strategy. The puissance losses and power contrivance costs are compared among the H5, the HERIC, and the proposed H6 topologies. A macrocosmic prototype is built for these three topologies mentioned for evaluating their performances in terms of puissance efficiency and leakage currents characteristics. Experimental results show that the proposed H6 topology and the HERIC achieve homogeneous performance in leakage currents, which is remotely worse than that of the H5 topology, but it features higher efficiency than that of H5 topology.

KEYWORDS—Common-mode voltage, grid-tied inverter, leakage current, photovoltaic (PV) generation system, transformer less inverter.

I. INTRODUCTION

THE applications of distributed photovoltaic (PV) generation systems in both commercial and residential structures have rapidly incremented during recent years. Albeit the price of PV panel has been declined largely, the overall cost of both the

investment and generation of PV grid-tied system are still too high, comparing with other renewable energy sources. Therefore, the grid-tied inverters need to be meticulously designed for achieving the purposes of high efficiency, low cost, minuscule size, and low weight, especially in the low-power single-phase systems (less than 5 kW). From the safety perspective, most

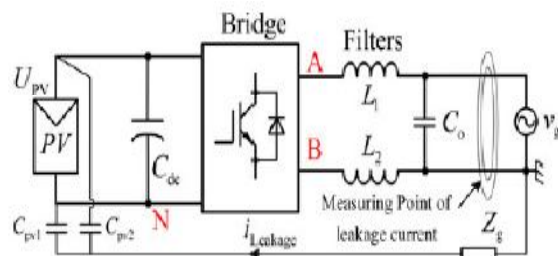


Fig. 1. Leakage current path for transformer less PV inverters.

the PV grid-tied inverters employ line-frequency transformers to provide galvanic isolation in commercial structures in the past. However, line-frequency transformers are immensely colossal and cumbersome, making the whole system bulky and hard to install. Compared with line-frequency isolation, inverters with high-frequency isolation transformers have lower cost, more minuscule size and weight. However, the inverters with high-frequency transformers have several power stages, which increase the system intricacy and reduce the system efficiency [1]–[6]. As a result, the transformer less PV grid-tied inverters, as shown in Fig. 1, are widely installed in the low-power distributed PV generation systems. Unfortunately, when the transformer is abstracted, the mundane mode (CM) leakage currents ($i_{leakage}$) may appear in the system and permeate the parasitic capacitances between the

PV panels and the ground [7], [8]. Moreover, the leakage currents lead to solemn safety and radiated interference issues [9]. Therefore, they must be constrained within a plausible range [10]. As shown in Fig. 1, the leakage current $I_{Leakage}$ is permeating the loop consisting of the parasitic capacitances (CPV1 and CPV2), bridge, filters (L_1 and L_2), utility grid, and ground impedance Z_g . The leakage current path is equipollent to an LC resonant circuit in series with the CM voltage [11], and the CM voltage v_{CM} is defined as

$$V_{CM} = \frac{V_{AN} + V_{BN}}{2} + (V_{AN} - V_{BN}) \frac{L_2 - L_1}{2(L_1 + L_2)} \quad (1)$$

where v_{AN} is the voltage difference between points A and N, v_{BN} is the voltage difference between points B and N. L_1 and L_2 are the output filter inductors. In order to eliminate leakage currents, the CM voltage must be kept constant or only varied at low frequency, such as 50 Hz/60 Hz. The conventional solution employs the half-bridge inverter [12], [13]. The filter inductor L_2 is zero in the half bridge inverters. Therefore, (1) is simplified as

$$V_{CM} = \frac{V_{AN} + V_{BN}}{2} - \left(\frac{V_{AN} - V_{BN}}{2} \right) = V_{BN} \quad (2)$$

The CM voltage v_{CM} is constant due to the neutral line of the utility grid connecting to the midpoint of the split dc-link capacitors directly. However, a drawback of half-bridge inverters is that, the dc voltage utilization of half-bridge type topologies is half of the full-bridge topologies. As a result, either large numbers of PV panels in series are involved or a boost dc/dc converter with extremely high voltage transfer ratio is required as the first power conditioning stage, which could decrease the system efficiency. The full-bridge inverters only need half of the input voltage value demanded by the half-bridge topology, and the filter inductors L_1 and L_2 are usually with the same value. As a result, (1) is simplified as

$$V_{CM} = \frac{V_{AN} + V_{BN}}{2} \quad (3)$$

Many solutions have been proposed to realize CM voltage constant in the full-bridge transformer less

inverters [14]–[25]. A traditional method is to apply the full-bridge inverter with the bipolar sinusoidal pulse width modulation (SPWM). The CM voltage of this inverter is kept constant during all operating modes. Thus, it features excellent leakage currents characteristic. However, the current ripples across the filter inductors and the switching losses are likely to be large. The full-bridge inverters with unipolar SPWM control are attractive due to the excellent differential-mode (DM) characteristics such as smaller inductor current ripple, and higher conversion efficiency. However, the CM voltage of conventional unipolar SPWM full bridge inverter varies at switching frequency, which leads to high leakage currents [12]. Two solutions could be applied to solve this quandary. One solution is to connect the PV negative terminal with the neutral line of the utility grid directly, such as the Karschny inverter derived from buck-boost converter [15], and the inverters derived from virtual dc-bus concept [16]. The CM voltage is kept constant by these full-bridge topologies with unipolar modulation methods. Another solution is to disconnect the dc and ac sides of the full-bridge inverter in the free wheeling modes. Sundry topologies have been developed and researched predicated on this method for keeping the CM voltage constant, such as the H5 topology [17], the highly efficient and reliable inverter concept (HERIC) topology [18], the H6-type topology [19], and the hybrid-bridge topology [20], etc., are shown in Fig. 2. Fig. 2(a) shows the H5 topology. It employs an extra switch on the dc side of inverter. As a result, the PV array is disconnected from the utility grid when the inverter output voltage is at zero voltage level, and the leakage current path is cut off. The HERIC topology shown in Fig. 2(b) employs two extra switches on the ac side of inverter, so the leakage current path is cut off as well. However, its power contrivance cost is higher than that of the H5 topology. Fig. 2(c) and (d) shows the H6-type topology and the hybrid-bridge topology respectively. Comparing with a full-bridge inverter, two extra switches are employed in the dc sides of these two topologies. Furthermore, both the H5 topology and the HERIC topology have been compared in terms of efficiency and leakage currents

characteristic [22]. However, these topologies have never been analyzed from the perspective of topological relationships. In this paper, a family of novel H6 full-bridge topologies is proposed for the transformer less PV grid-tied inverters. An extra

switch is inserted to the H5 topology for composing an incipient current path and for the purport of reducing conduction loss. There fore ,in the active modes, the inductor current of the proposed H6 topology permeates two switches during one of the moiety line periods and through three switches during another half-line period. As a result, for comparing with the topologies presented in [17], [19], and [20], the proposed H6 topology has achieved the minimum conduction loss, and withal has featured with low leakage currents. On the other hand, the topological relationship between H5 topology and HERIC topology is revealed, and the methods for engendering HERIC topology from H6-type topology and from hybrid-bridge topology are presented, respectively. This paper is organized as follows. In Section II, the operation modes and characteristics of the H5 topology and the HERIC topology are presented and compared. The methods of

engendering HERIC topology from the H6-type topology or from the hybrid-bridge topology are given. A family of H6 topologies is proposed, and the topological relationship between H5 topology and HERIC topology is analyzed. In Section III, one of the proposed H6 topologies is taken as an example for analysis in detail with operational principle and modulation strategy. The comparisons between H5, HERIC, and the proposed H6 topology are given in terms of potency loss and contrivance cost. Experimental results are presented in Section IV, and Section V concludes the paper.

III. ANALYSIS ON THE H6 TOPOLOGY AND COMPARISON WITH OTHER TOPOLOGIES

A. Novel H6 Topology

From the aforementioned analysis, an extra switch S6 is introduced into the H5 inverter topology between the positive terminal of the PV array and the terminal (B) to form a new

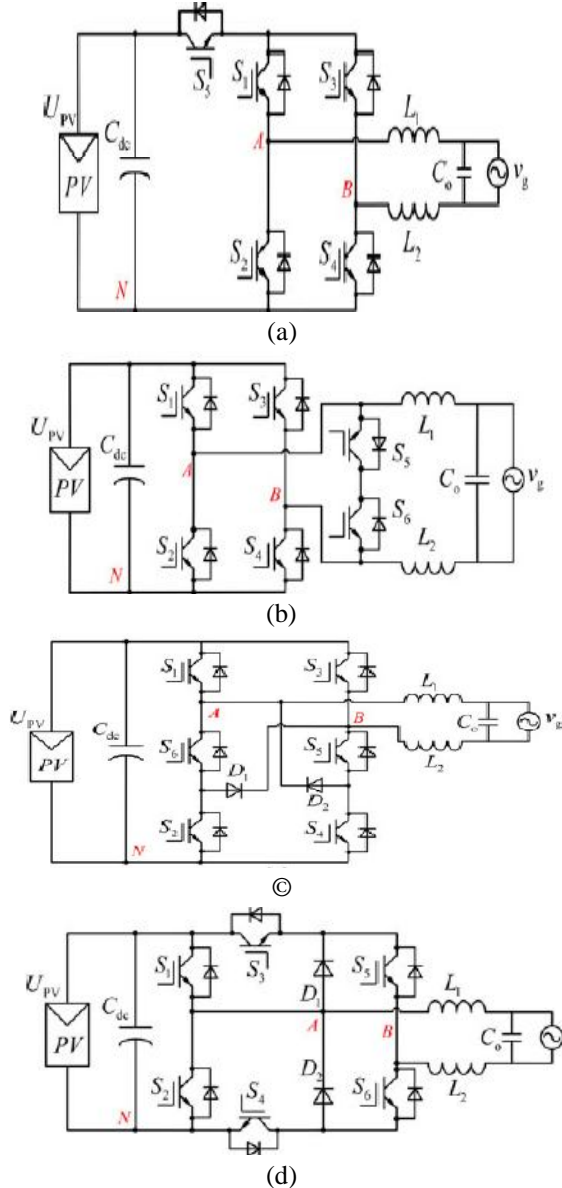
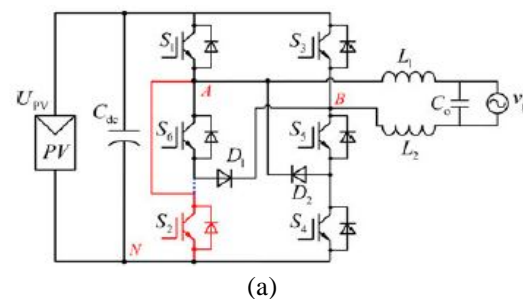


Fig. 2. Four typical topologies of transformer less full-bridge inverters.(a). H5. (b) HEIRC. (c) H6-type. (d) Hybrid bridge.

switch is inserted to the H5 topology for composing an incipient current path and for the purport of reducing conduction loss. There fore ,in the active



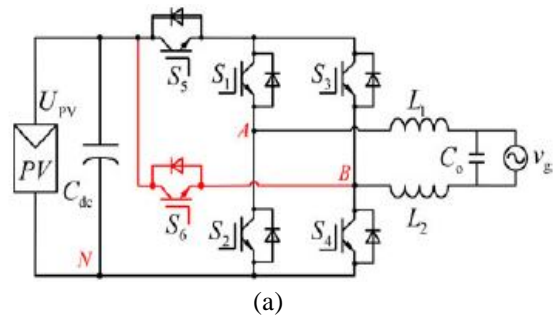
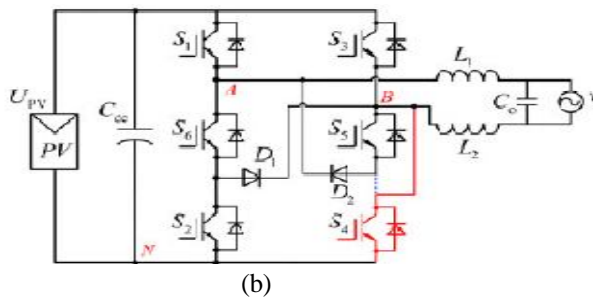


Fig. 3. Modified H6-type inverter topologies. (a) Circuit structure A. (b) Circuit structure B.

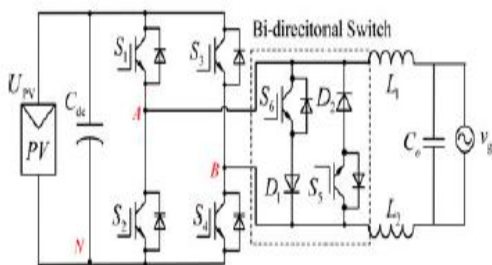


Fig. 4. Another circuit structure of HERIC topology.

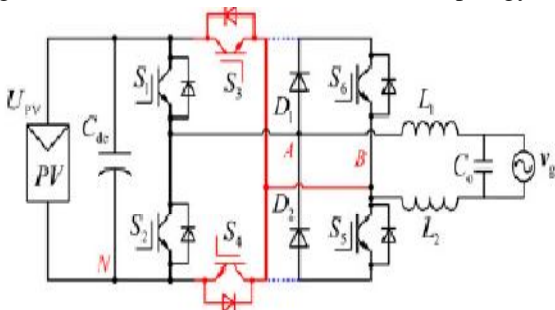


Fig. 5. Another circuit structure of HERIC topology derived from hybrid bridge topology.

current path. As a result, a novel H6 transformer less full-bridge inverter topology is derived, as shown in Fig. 9(a).

Similarly, the extra switch S6 can be introduced into the H5 inverter topology between the positive terminal of the PV array and the terminal (A) to compose an incipient current path as well, as shown in Fig. 9(b). Therefore, an incipient circuit structure of novel H6 inverter is presented. As a result, the conduction loss of the proposed H6 topologies is higher than HERIC topology and less than H5 topology.

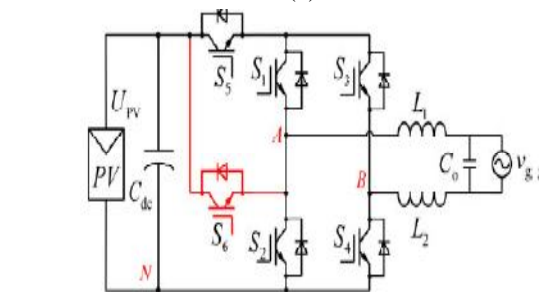


Fig. 6. A family of proposed H6-type inverter topologies. (a). Circuit structure A. (b) Circuit structure B.

B. Operation Mode Analysis

The circuit structure of proposed novel H6 inverter topologies shown in Fig. 9(a) is taken as an example to analysis. PV grid-tied systems usually operate with unity power factor. The waveforms of the gate drive signals for the proposed novel H6 topology are shown in Fig. 10, where v_g is the voltage of utility grid. i_{ref} is the inductor current reference. v_{gs1} to v_{gs6} represent the gate drive signals of switches S1 to S6, respectively. There are four operation modes in each period of the utility grid, as shown in Fig. 11, where v_{AN} represents the voltage between terminal (A) and terminal (N) and v_{BN} represents the voltage between terminal (B) and terminal (N). v_{AB} is the DM

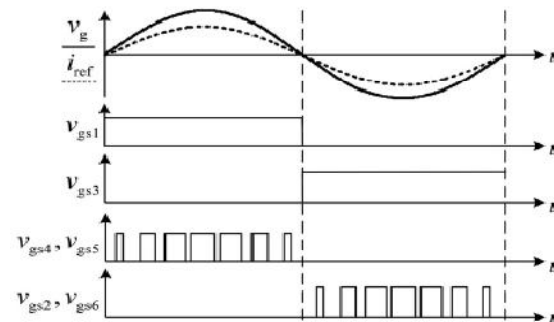


Fig. 7. Schematic of gate drive signals with unity power factor.

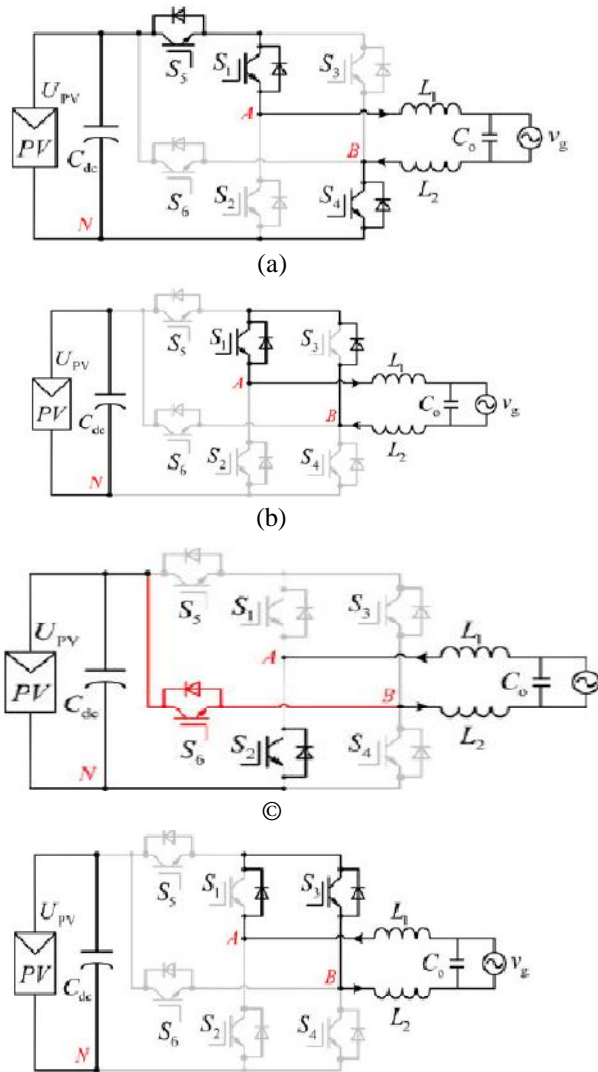


Fig .8. Equivalent circuits of operation modes. (a)Active mode in the positive half period. (b) Freewheeling mode in the positive half period. (c) Active mode in the negative half period. (d) Freewheeling mode in the negative half period.

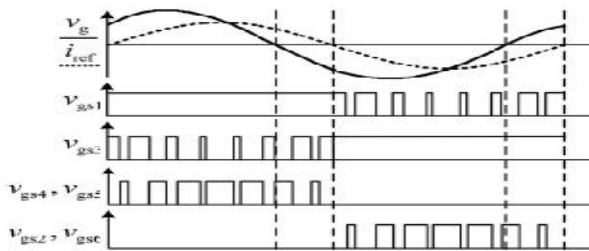


Fig. 9. Schematic of gate drive signals with power factor other than unity.

voltage of the topology, $v_{AB} = v_{AN} - v_{BN}$. The CM voltage $v_{CM} = 0.5(v_{AN} + v_{BN})$.

a) Mode I is the active mode in the positive half period of the utility grid voltage, as shown in Fig. 11(a). S_1, S_4 , and S_5 are turned ON, and the other switches are turned OFF. The inductor current is flowing through S_1, S_4 , and S_5 . $v_{AN} = UPV$, $v_{BN} = 0$; thus, $v_{AB} = UPV$, and the CM voltage $v_{CM} = (v_{AN} + v_{BN})/2 = 0.5UPV$.

b) Mode II is the freewheeling mode in the positive half period of the utility grid voltage, as shown in Fig. 11(b). S_1 is turned ON; the other switches are turned OFF. The inductor current is flowing through S_1 and the anti parallel diode of S_3 . $v_{AN} = v_{BN} \approx 0.5UPV$; thus, $v_{AB} = 0$, and the CM voltage $v_{CM} = (v_{AN} + v_{BN})/2 \approx 0.5UPV$.

c) Mode III is the active mode in the negative half period of the utility grid voltage, as shown in Fig. 11(c). S_2, S_3 , and S_6 are turned ON; the other switches are turned OFF. The inductor current is flowing through S_2 and S_6 . Although S_3 is turned ON, there is no current flowing through it, and the switch S_3 has no conduction loss in this mode. Nevertheless, in the H5 topology, the inductor current flows through S_2, S_3 , and S_5 . Therefore, the conduction loss of proposed topology is less than that of H5 topology. In this mode, $v_{AN} = 0$, $v_{BN} = UPV$; thus, $v_{AB} = -UPV$, and the CM voltage $v_{CM} = (v_{AN} + v_{BN})/2 = 0.5UPV$.

d) Mode IV is the freewheeling mode in the negative half period of the utility grid voltage, as shown in Fig. 11(d). S_3 is turned ON, and the other switches are turned OFF. The inductor current is flowing through S_3 and the anti parallel diode of S_1 . $v_{AN} = v_{BN} \approx 0.5UPV$; thus, $v_{AB} = 0$, and the CM voltage $v_{CM} = (v_{AN} + v_{BN})/2 \approx 0.5UPV$.

Based on the aforementioned analysis, the PV array can be disconnected from the utility grid when the output voltage of the proposed H6 inverter is at zero voltage level and the leakage current path is cut off. The CM voltage of the proposed topology in each operation mode is equals to $0.5UPV$, and it results in low leakage current characteristic of the proposed H6 topologies. The proposed H6 topology with unipolar SPWM method not only can achieve unity power

factor, but also has the ability to control the phase shifts between voltage and current waveforms.

The modulation strategy is shown in Fig. 12. The drive signal is in phase with the grid-tied current.

TABLE I

CALCULATED POWER LOSSES ON DEVICE

	S ₁ (W)	S ₂ (W)	S ₃ (W)	S ₄ (W)	S ₅ (W)	S ₆ (W)	Total losses(W)
H5	4.911	4.472	4.911	4.472	8.944	N.C.	27.71
HEIRC	4.472	4.472	4.472	4.472	2.571	2.571	23.03
H6	4.911	4.472	2.571	4.472	4.472	4.472	25.37

Fig. 13. Device losses distribution for these three topologies with 1 kW power rating.

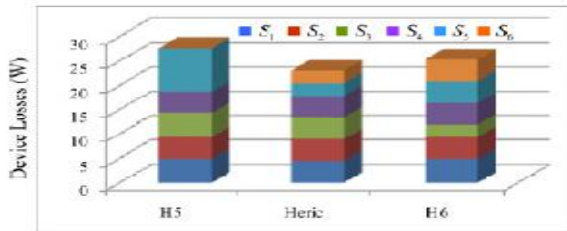


TABLE II

COMPARISON OF OPERATING DEVICES IN THESE THREE TOPOLOGIES

	H5	HERIC	H6
Total device number	5	6	6
Isolated power supply for devices	4	3	4
Switching device number	2	2	2
Conducting device number	$v_{ic} > 0$	3	2
	$v_{ic} < 0$	3	2
Diodes number with freewheeling	2	2	2
Diodes number with reverse recovery	1	1	1
Gate drive number	2	2	2

C. Comparisons of H5, HERIC, and the Proposed H6Topologies

The power losses of power switches of the proposed H6 topology[see Fig. 9(a)], H5 topology [see Fig. 2(a)], and HERIC topology [see Fig. 2(b)], are calculated with the same parameters as given in Table III, and are illustrated in Table I and Fig. 13.The calculation methods and theories are studied and verified

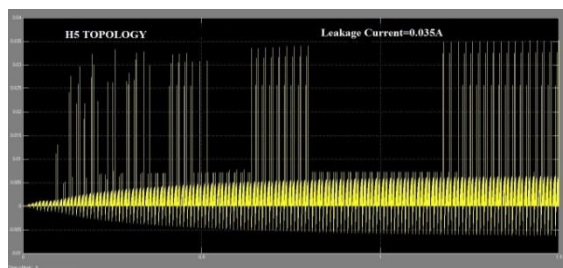


Fig. 10. Simulation results for the H5topology Leakage currents

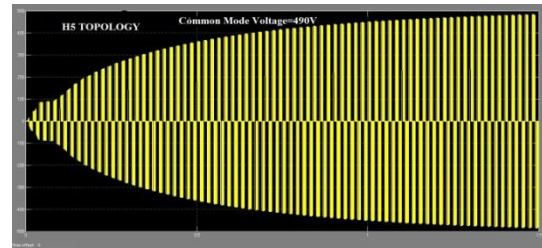


Fig. 11. Simulation results for the H5topology

Common mode voltages

in detail in literatures [22], [26]–[29], but not the contribution of this paper. On the other hand, the inductor losses in the three topologies are identically tantamount due to the same vAB modulation. Therefore ,the inductor losses of these three topologies are regardless .The comparison of operating contrivances in these three topologies are summarized in Table II. The main power losses of switches in each operation mode include the turn-ON/OFF loss, conduction

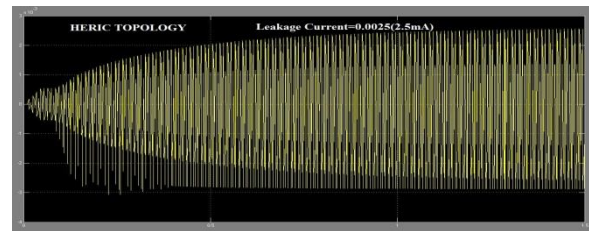
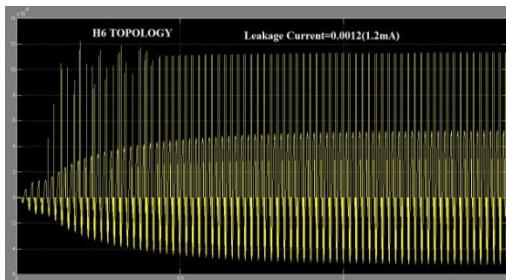


Fig. 12. Simulation results for the HERIC topology Leakage currents

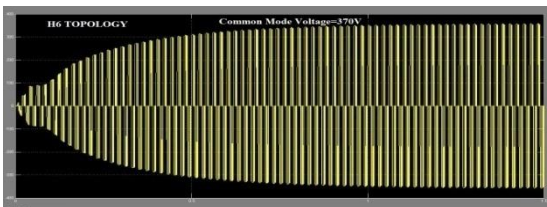
From Tables I and II, it can be visually perceived that the H5 topology only has five power contrivances. Thus, it has the lowest contrivance cost. The contrivance cost of HERIC and H6 is equipollent. The switching loss ,diode freewheeling loss, diode reverse instauration loss, and gate drive loss of these three topologies are equipollent. However, H5topology has the highest conduction loss, and the conduction loss of the proposed H6 is higher than that of the HERIC topology .From Fig. 13, it can be optically discerned that HERIC topology has the best thermal stress distribution, while the H5 topology is the worst. The potency loss of HERIC topology is the lowest.

A macrocosmic prototype of H5 [see Fig. 2(a)], HERIC [seeFig. 2(b)], and novel H6 [see Fig. 9(a)] topologies has been built up in order to verify the

operation principle and compare their performances. The designations of these three inverter topologies are listed in Table III. The control circuit is implemented predicated on a DSP chip TMS320F2808. The quantification point of leakage currents is shown in Fig. 1. Because Z_g is diminutively minuscule, it is not being considered. The picture for the macrocosmic prototype is depicted in Fig. 14. The YOKOGAWA WT1800 precision



(a)



(b)

Fig. 13. CM voltage and leakage current in H6 topology. (a) CM voltage.(b) Leakage current.

power analyzer was utilized as the measurement instrument to measure the efficiency of these three different topologies. The CM voltage and the leakage current waveforms of these three topologies in unified experimental conditions are shown in Figs. 15–17, respectively, where v_g and i_g are the grid voltage and grid-tied current, respectively. v_{AN} and v_{BN} are the voltages between the midpoints A and B to terminal N, respectively. v_{CM} is the CM voltage, which equals to $0.5(v_{AN} + v_{BN})$. $I_{leakage}$ represents the leakage current. The leakage current measured for the H5, HERIC, and H6 inverters at the switching frequency are 6 mA [see Fig. 15(b)], 9 mA [see Fig. 16(b)], and 9 mA [see Fig. 17(b)], respectively. The fast Fourier transform (FFT) results show that the leakage current of H5 topology is the lowest, and the leakage current of HERIC topology

and H6 topology is almost the same. The drain–source voltage waveforms of switches in the novel H6 topology are shown in Fig. 18, where v_{ds5} and v_{ds6} are drain–source voltages of S5 and S6, respectively. From Fig. 18(b), it can be seen that in the negative half period of the utility grid voltage, the voltage potential of the positive terminal of the PV array is equal to that of the terminal (B), so the drain–source voltage of switch S5 is zero. Thus, the switch S5 only has switching loss in the positive half period. As a result, the switching loss of H5 topology and the proposed H6 topology is the same. The experimental results agree closely with the results from theoretical analysis. Due to the freewheeling path disconnected from the PV array in the freewheeling modes, the ringing of the voltage envelopes of S5 and S6 depends on the parasitic parameters of the leakage current path and the utility grid voltage amplitude.

Fig. 14 shows the DM characteristic of the proposed H6 topology, where v_{AB} is the DM voltage. It can be seen that

the output voltage v_{AB} has three levels as UPV, 0, and $-UPV$, which indicates that the proposed H6 topology employs unipolar SPWM as modulation strategy, and the DM characteristic is excellent.

Fig. 14 is the conversion efficiency comparison of H5, HERIC, and H6 topologies under the same condition. It is obvious that the efficiency of the HERIC is the highest and that the efficiency of the proposed H6 topology takes the second place. The experimental results are in agreement with the power losses analysis in Section III-B. The European efficiencies of H5, HERIC, and H6 are 96.78%, 97%, and 97.09%, respectively.

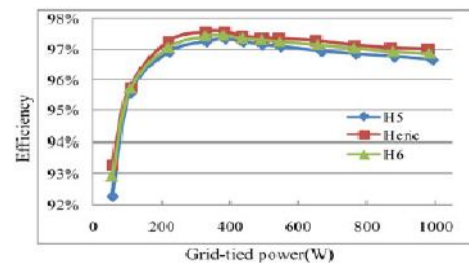


Fig. 14. Efficiency comparison of H5, HERIC and H6 topologies.

In summary, the H5 topology has the best leakage current characteristic, but its efficiency is the lowest. The HERIC topology has the highest efficiency, but the leakage current characteristic is worse than that of H5 topology. The leakage current characteristic of proposed H6 topology is virtually identically tantamount to that of HERIC topology. The efficiency of proposed H6 topology is a little less than the HERIC topology, but it is higher than H5 topology.

V. CONCLUSION

In this paper, from the topological relationship perspective, the intrinsic relationship between H5 topology and HERIC topology is revealed. The HERIC topology can be derived from H5, H6-type, and hybrid-bridge topologies by the conception of reducing conduction loss. Moreover, predicated on the H5 topology, an incipient current path is composed by inserting a potency contrivance between the terminals of PV array and the midpoint of one of bridge legs. As a result, a family of single-phase transformer less full-bridge H6 inverter topologies with low leakage currents is derived. The proposed H6 topologies have the following advantages and evaluated by experimental results:

- 1) the conversion efficiency of the novel H6 topology is better than that of the H5 topology, and its thermal stress distribution is better than that of the H5 topology;
- 2) the leakage current is virtually equipollent to HERIC topology, and meets the safety standard;
- 3) the excellent DM performance is achieved like the isolated full-bridge inverter with unipolar SPWM. Therefore, the proposed H6 topologies are good solutions for the single phase transformer less PV grid-tied inverters.

REFERENCES

[1] S. B. Kjaer, J. K. Pederson, and F. Blaabjerg, "A review of single-phase grid-connected inverters for photovoltaic modules," *IEEE Trans. Ind. Appl.*, vol. 41, no. 5, pp. 1292–1306, Sep/Oct. 2005.

[2] F. Blaabjerg, Z. Chen, and S. B. Kjaer, "Power electronics as efficient interface in dispersed power generation systems," *IEEE Trans. Power Electron.*, vol. 19, no. 5, pp. 1184–1194, Sep. 2004.

[3] B. Sahan, A. N. Vergara, N. Henze, A. Engler, and P. Zacharias, "A single stage PV module integrated converter based on a low-power current source inverter," *IEEE Trans. Ind. Electron.*, vol. 55, no. 7, pp. 2602–2609, Jul. 2008.

[4] M. Calais, J. Myrzik, T. Spooner, and V. G. Agelidis, "Inverters for single phase grid connected photovoltaic systems—An overview," in *Proc. IEEE PES*, 2002, vol. 2, pp. 1995–2000.

[5] F. Blaabjerg, Z. Chen, and S. B. Kjaer, "Power electronics as efficient interface in dispersed power generation systems," *IEEE Trans. Power Electron.*, vol. 19, no. 5, pp. 1184–1194, Sep. 2004.

[6] Q. Li and P. Wolfs, "A review of the single phase photovoltaic module integrated converter topologies with three different dc link configuration," *IEEE Trans. Power Electron.*, vol. 23, no. 3, pp. 1320–1333, May 2008.

[7] O. Lopez, F. D. Freijedo, A. G. Yepes, P. Fernandez-Comesana, J. Malvar, R. Teodorescu, and J. Doval-Gandoy, "Eliminating ground current in a transformerless photovoltaic application," *IEEE Trans. Energy Convers.*, vol. 25, no. 1, pp. 140–147, Mar. 2010.

[8] R. Gonzalez, J. Lopez, P. Sanchis, and L. Marroyo, "Transformerless inverter for single-phase photovoltaic systems," *IEEE Trans. Power Electron.*, vol. 22, no. 2, pp. 693–697, Mar. 2007.

[9] H. Xiao and S. Xie, "Leakage current analytical model and application in single-phase transformerless photovoltaic grid-connected inverter," *IEEE Trans. Electromagn. Compat.*, vol. 52, no. 4, pp. 902–913, Nov. 2010.

[10] VDE-AR-N 4105: *Power Generation Systems Connected to the Low-Voltage Distribution Network—Technical Minimum Requirements For the Connection to and Parallel Operation with Low-Voltage Distribution Networks*, DIN_VDE Normo, 2011–08.

[11] B. Yang, W. Li, Y. Gu, W. Cui, and X. He, "Improved transformerless inverter with common-mode leakage current elimination for a photovoltaic grid-connected power system," *IEEE Trans. Power Electron.*, vol. 27, no. 2, pp. 752–762, Feb. 2012.

[12] R. Gonzalez, E. Gubia, J. Lopez, and L. Marroyo, "Transformerless single phase multilevel-based photovoltaic inverter," *IEEE Trans. Ind. Electron.*, vol. 55, no. 7, pp. 2694–2702, Jul. 2008.

- [13] H. Xiao and S. Xie, "Transformerless split-inductor neutral point clamped three-level PV grid-connected inverter," *IEEE Trans. Power Electron.*, vol. 27, no. 4, pp. 1799–1808, Apr. 2012.
- [14] L. Zhang, K. Sun, L. Feng, H. Wu, and Y. Xing, "A family of neutral point clamped full-bridge topologies for transformerless photovoltaic grid-tied inverters," *IEEE Trans. Power Electron.*, vol. 28, no. 2, pp. 730–739, Feb. 2012.
- [15] German Patent Wechselrichter: DE 19642522C1 Apr. 1998.
- [16] Y. Gu, W. Li, Y. Zhao, B. Yang, C. Li, and X. He, "Transformerless inverter with virtual DC bus concept for cost-effective grid-connected PV power systems," *IEEE Trans. Power Electron.*, vol. 28, no. 2, pp. 793–805, Feb. 2012.
- [17] M. Victor, F. Greizer, S. Bremicker, and U. Hübner, "Method of converting a direct current voltage from a source of direct current voltage, more specifically from a photovoltaic source of direct current voltage, into an alternating current voltage," U.S. Patent 7 411 802, Aug. 12, 2008.
- [18] S. Heribert, S. Christoph, and K. Jürgen, "Inverter for transforming a DC voltage into an AC current or an AC voltage," Europe Patent 1 369 985(A2), May 13, 2003.
- [19] W. Yu, J. Lai, H. Qian, and C. Hutchens, "High-efficiency MOSFET inverter with H6-type configuration for photovoltaic nonisolated ac-module applications," *IEEE Trans. Power Electron.*, vol. 26, no. 4, pp. 1253–1260, Apr. 2011.